Journal of the European Ceramic Society xxx (xxxx) xxx–xxx

Contents lists available at ScienceDirect

Journal of the European Ceramic Society

journal homepage: www.elsevier.com/locate/jeurceramsoc

Original Article

Design of Lu_2O_3-reinforced C_f/SiC-ZrB_2-ZrC ultra-high temperature ceramic matrix composites: Wetting and interfacial reactivity by $ZrSi_2$ based alloys

Peter Tatarko[a,*], Fabrizio Valenza[b], Hakan Ünsal[a], Alexandra Kovalčíková[c], Jaroslav Sedláček[a], Pavol Šajgalík[a]

[a] Institute of Inorganic Chemistry, Slovak Academy of Sciences, Dúbravská Cesta 9, 845 36, Bratislava, Slovakia
[b] Institute of Condensed Matter Chemistry and Technologies for Energy - ICMATE, National Research Council –CNR, Via De Marini 6, 161-49 Genoa, Italy
[c] Institute of Materials Research, Slovak Academy of Sciences, Watsonová 47, 040 01 Košice, Slovakia

ARTICLE INFO

Keywords:
Ultra-High temperature ceramics
Ceramic matrix composites
Wettability
Zirconium silicide
Reactive melt infiltration

ABSTRACT

The wettability and infiltration of molten $ZrSi_2$ and $ZrSi_2$-Lu_2O_3 alloys into C_f/SiC and B_4C-infiltrated C_f/SiC composites were investigated to understand the interfacial interactions that occur during the development of C_f/SiC-ZrC and C_f/SiC-ZrB_2-ZrC-Lu_2O_3 materials. A significant evaporation of Si from the liquid affected the wetting behaviour of the alloy when tested in a vacuum at 1670 °C. The better wetting and spreading of the alloy over the surface was observed for the composites with lower overall porosity (12 %). On the other hand, the formation of an outer dense layer, followed up by the uniform infiltrated region up to ~ 1 mm was observed for the C_f/SiC with higher porosity (21 %). The infiltrated alloy reacted with SiC matrix to form ZrC or with B_4C-infiltrated SiC matrix to form ZrB_2-ZrC-SiC. The Lu_2O_3 particles were not wetted by the melt, and were pushed away of the reaction zone by the solidification front.

1. Introduction

Development of new low-cost space launch systems and hypersonic vehicles requires advanced materials for Thermal Protection Systems (TPS) with temperature capabilities well above 2000 °C, as hypersonic vehicles with velocities above Mach 5 experience high aerodynamic and thermo-chemical loads on their surface [1–3]. Ceramic Matrix Composites (CMCs), such as C_f/C and C_f/SiC, are materials of great interest for aerospace applications, including TPS, aero-engine parts, and hot gas valve parts, due to their superior mechanical properties, damage tolerance and light weight [4]. However, their maximum temperature application is limited to 1600 °C in an oxygen-rich environment, or 1800 °C in a low oxygen atmosphere [5]. There is an increasing interest in improving the capability of current CMCs to withstand harsh environmental conditions [6]. Transition metal compounds with extremely high melting points (so called “ultra-high temperature ceramics – UHTCs”), particularly borides of Zr and Hf – ZrB_2 and HfB_2, are considered as the alternative materials for TPS and other demanding aerospace applications [1]. Their application is also limited due to the low thermal shock resistance, lack of flaw tolerance and relatively high density.

In recent years, therefore, a new class of materials, so called Ultra-High Temperature Ceramic Matrix Composites (UHTCMCs), has been developed by the combination of CMCs and UHTCs in order to utilize both the high mechanical reliability of CMCs and the ultra-high properties of UHTCs into one material system [6,7]. In such a way, problems arising from the brittleness and low thermal shock resistance of UHTCs, and the limited oxidation resistance of CMCs can be mitigated. Several techniques have been used to produce this class of materials, including slurry infiltration and Chemical Vapour Infiltration (CVI) [8], slurry infiltration and Hot Pressing (HP) [7], slurry infiltration and Spark Plasma Sintering (SPS) [9], Polymer Infiltration and Pyrolysis (PIP) [10], or Reactive Melt Infiltration (RMI) [11,12]. Among these techniques, RMI has attracted attention because of great advantages that lie in a fast densification and low cost. RMI technique has been successfully used either to infiltrate C_f preforms with molten Zr to form C_f/C-ZrC composites [13], or C_f/B_4C-C preforms with molten $ZrSi_2$ alloy to form C_f/SiC-ZrB_2-ZrC composites [12,14], or C_f preforms with molten Zr-B eutectic to form C_f/ZrC-ZrB_2 composites [15]. RMI has also been used in combination with PIP to produce 3D C_f/ZrC-SiC composites, in which a molten Zr-Si alloy was infiltrated into the C_f/C-SiC substrate, prepared by PIP [16]. Similarly, CVI combined with RMI of Zr-Si alloy was used to develop C_f/C-ZrC composites [17].

During the fabrication of UHTCMCs by RMI, a UHTC matrix is

* Corresponding author.
E-mail addresses: peter.tatarko@savba.sk, tatarko.peter@gmail.com (P. Tatarko).

https://doi.org/10.1016/j.jeurceramsoc.2020.05.055
Received 1 March 2020; Received in revised form 7 May 2020; Accepted 22 May 2020

obtained through the in-situ reactions between a reactive alloy melt and active filler inside the preform. An alloy is infiltrated into preforms under the driving force of capillary pressure, if the contact angle at the pore walls is significantly lower than 90° [18,19]. At the same time, RMI process is significantly affected by the preform structure (porosity, pore size), viscosity of the alloy, infiltration temperature, and atmosphere. However, it is rather difficult to identify and control the interfacial phenomena occurring at the metal/ceramic interfaces, because diffusion and reaction may concur, or even compete with wettability [20]. These interactions may cause interfacial instability, decomposition of a reinforcement phase, or the presence of brittle interfacial reaction compounds, which all can deteriorate the thermo-mechanical properties of the composites. It has been reported that the presence of Zr-species in the melt results in a strong corrosive medium, which causes a significant erosion of C fibres in the final composites [11,12]. One way of avoiding the undesired degradation of the materials is to protect carbon fibres with an inert interface, such as SiC or BN [20]. Therefore, in order to design and manufacture new types of UHTCMCs, it is extremely important to investigate the wetting and reactivity behaviour of a molten alloy on the CMC materials at different conditions. Despite this, only a few recent studies have been focused on the wetting and infiltration behaviour of molten Zr-based alloys, e.g. $ZrSi_2$ in contact with C_f/B_4C-C preform [11], or Si-10Zr and $Si_{0.92}Zr_{0.08}$ alloys on SiC substrates [20,21]. On the other hand, no wetting and interfacial investigation of molten Zr-Si alloy on C_f/SiC substrate has been reported. Such a study might be of a great interest because the carbon fibres are protected against the effect of reactive Zr-Si alloy by the surrounding SiC matrix. This is expected to lead to the significantly improved overall performance of the final UHTCMC composites, when compared to the infiltration of molten Zr-Si alloy into C_f preforms, in which carbon fibres are just covered by active fillers (PyC, B_4C, SiC, etc).

It was the aim of the present work to investigate the wetting and interfacial reactivity of molten $ZrSi_2$-based alloys on C_f/SiC substrates with two different porosities prepared by PIP. The current paper proposes a new type of UHTCMC material, in which a C_f/SiC matrix is reinforced with the in-situ formed ultra-high temperature phase ZrB_2-SiC-ZrC-Lu_2O_3 by reactions of molten $ZrSi_2$ – 5 wt.% Lu_2O_3 alloy with the B_4C-infiltrated C_f/SiC substrate. In the first step, the wettability and reactivity of pure molten $ZrSi_2$ alloy in contact with CVD-SiC and C_f/SiC substrates were investigated to understand the effect of ambient atmosphere (vacuum or argon) and porosity of the matrix. The CVD-SiC was used to study the interfacial reactivity and the liquid distribution of molten $ZrSi_2$ over the SiC surfaces without the effect of porosities and surface roughness, typical of CMCs. In the second step, the wetting and infiltration of $ZrSi_2$ – 5 wt.% Lu_2O_3 alloy on the B_4C-infiltrated C_f/SiC substrates were investigated. The addition of Lu_2O_3 was used to further improve refractoriness of the in-situ formed UHTC matrix in the C_f/SiC composites. It has been reported that the addition of rare-earth oxides (RE_2O_3) into the UHTCs may lead to the improved oxidation resistance, due to the formation of refractory pyrochlore $RE_2Me_2O_7$ phase (where RE is a rare earth element, and Me is Zr or Hf) with melting temperatures above 2200 °C [22–25]. During oxidation, RE oxides react with the oxidation products of ZrB_2 and HfB_2 to form phases with a pyrochlore structure. Their presence in the in-situ formed oxide layer increases immiscibility (also known as phase separation) and viscosity of the glassy layer, leading to the reduced oxygen diffusion rate through the oxide layer [22]. In addition, the immiscibility and viscosity of the in-situ formed glass phase (during the oxidation of diborides) increase with decreasing size of RE^{3+} cations, due to the increased cation field strength (CFS) [23,24]. The extraordinary effect of RE element with the smallest RE^{3+} cation (Lu^{3+}) was reported to significantly improve the oxidation resistance and other high temperature properties of silicon nitride [26,27]. However, such an additive has never been used to reinforce UHTCs and/or UHTCMCs. In addition, rare earth oxides have been primarily used in UHTC materials based on Zr- or Hf-diborides [22–24], but only several works have been focused on the utilization of RE (mainly La or Y) while producing UHTCMCs [25,28]. This is probably caused by more complex and difficult incorporation of RE elements into UHTCMCs, when compared to UHTC matrices.

This work was aimed to investigate the wettability and infiltration of molten $ZrSi_2$ and $ZrSi_2$-Lu_2O_3 alloys into C_f/SiC and B_4C-infiltrated C_f/SiC composites, thereby understanding the interfacial interactions that occur during the development of C_f/SiC-ZrC and C_f/SiC-ZrB_2-ZrC-Lu_2O_3 materials, respectively. To the best of our knowledge, this is the first time such a material system has been proposed and investigated.

2. Experimental procedure

2.1. Substrate materials

With the aim to determine the real interfacial behaviour between SiC and $ZrSi_2$ as a function of working atmosphere, the wetting experiments were first performed on the high purity (99.9995 at. %), fully dense (3.21 g/cm^3) Chemically Vapour Deposited (CVD) β-SiC substrates (The Dow Chemical Company, USA). The samples with dimensions of 10 × 10 × 4 mm^3 were used as the substrates. In order to avoid pinning phenomena at the drop triple line and to remove the oxide native layer, the substrates were polished with a 1 μm diamond paste to reach a surface roughness Sa = 4 nm, which was measured using an optical confocal profilometer (Sensofar S-neox) over a 1.75 × 1.32 mm^2 surface area.

The C_f/SiC substrates (supplied by Airbus Defence and Space GmbH, Germany) were manufactured using polymer impregnation and pyrolysis (PIP) of C_f preform. The carbon fibres were coated by a PyC layer (~ 400 nm). The samples consisted of 16 layers in alternating 0°/90° fibres orientation. Either 3 PIP cycles (C_f/SiC-I3) or 6 PIP cycles (C_f/SiC-I6) were employed to produce the final C_f/SiC composites with two different densities (1.84 g/cm^3 for C_f/SiC-I3; and 2.07 g/cm^3 for C_f/SiC-I6) and overall porosities (21 % for C_f/SiC-I3; 12 % for C_f/SiC-I6). The samples with the dimensions of 10 × 10 × 3 mm^3 were received from the supplier. The SEM microstructures of both as-

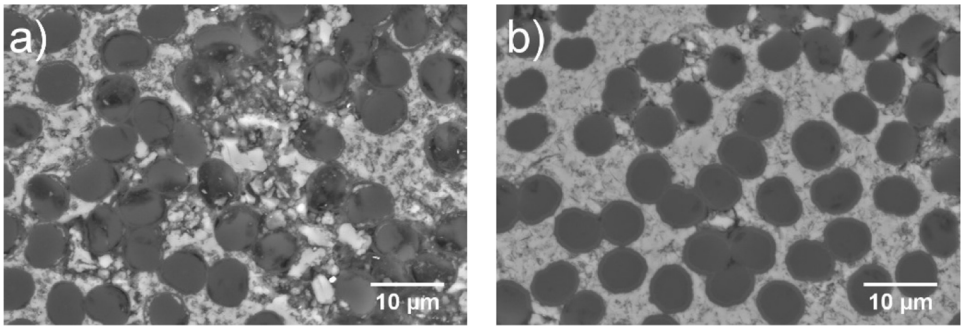

Fig. 1. Back-scattered SEM microstructures of the as-received C_f/SiC substrates manufactured by different number of PIP cycles: a) C_f/SiC-I3; b) C_f/SiC-I6.

Table 1
Summary of the material combinations investigated in the present work, along with the corresponding apparent contact angles (if measured) after the wetting tests at 1670 °C for 5 min.

Substrate	Pellet	Atmosphere	Angle
CVD SiC	$ZrSi_2$	Vacuum	50°
	$ZrSi_2$	Argon	38°
	$ZrSi_2$ - 5 wt.% Lu_2O_3	Argon	50°
C_f/SiC-I3	$ZrSi_2$	Vacuum	–
	$ZrSi_2$	Argon	–
C_f/SiC-I6	$ZrSi_2$	Vacuum	–
	$ZrSi_2$	Argon	23°
C_f/SiC-I3 + B_4C	$ZrSi_2$ - 5 wt.% Lu_2O_3	Argon	–
C_f/SiC-I6 + B_4C	$ZrSi_2$ - 5 wt.% Lu_2O_3	Argon	43°

received C_f/SiC samples are shown in Fig. 1. It can be clearly seen that a higher number of PIP cycles eliminated the small micropores and led to the microstructure with a less porous SiC matrix. No polishing or other surface treatment were employed prior the wetting tests.

In order to form a desired composition of ZrB_2-SiC in the surface layer, both C_f/SiC samples were infiltrated by B_4C powder using pressure infiltration. The B_4C powder (grade HD20, d50 ~ 0.3 – 0.6 μm, H.C. Starck, Germany) was used to prepare isopropanol-based suspension (solid loading of 4 vol. %). The C_f/SiC samples were submerged into the suspension and the B_4C slurry was infiltrated into the sample bodies by pressure infiltration using the pressure of 15 MPa for 20 min. This infiltration process was repeated 5 times. After each infiltration cycle, the samples were dried in an oven at 70 °C for 4 h. The weight gain after the last infiltration cycle was ~ 1 wt.% for the C_f/SiC-I_3 sample, while ~ 0.5 wt.% for the C_f/SiC-I6 samples. This indicates that a higher amount of B_4C was infiltrated into the sample with a higher open porosity (~ 18 %), when compared to the C_f/SiC-I6 sample with a lower open porosity (~ 9 %).

2.2. Alloys

Commercially available $ZrSi_2$ powder (ABCR GmbH, Germany) with the purity of 99.5 % and the average particle size of 2.12 μm, and Lu_2O_3 powder (Treibacher Industrie AG, Austria) with the purity of 99.99 % (d50 = 4.7 μm) were used as raw materials in this work. The powder mixture was prepared using a planetary ball mill (PM 100, Retsch) in a 250 mL WC jar with WC balls (Ø 10 mm) for 2 h at a speed of 250 rpm. The use of WC ball milling media led to the contamination of the powder mixture, which at the end contained ~ 2.1 wt.% WC (determined by Rietveld analysis). Both the pure $ZrSi_2$ powder and the $ZrSi_2$ + 5 wt.% Lu_2O_3 powder mixture were compacted into the pellets with dimensions of Ø 4 mm x 2 mm by Cold Isostatic Pressing (EPSI CIP 400 – 300 *750Y, Belgium) using the pressure of 400 MPa for 60 s. No further heat treatment of the pellets was performed before wetting tests.

2.3. Wetting experiments

To perform the wetting experiments the compacted pellets were placed onto the substrate surfaces and placed in a wetting apparatus. The equipment used for these tests consists of a furnace heated by a high-frequency generator coupled with a vitreous carbon susceptor [29]. The temperature was measured using an optical pyrometer, which was calibrated by melting a piece of pure iron (T_m = 1538 °C) before the tests. After setting up the samples and having assured a clean atmosphere by inserting pure Ar (Air Liquide, Alphagaz 2) and evacuating for three times, the samples were heated up and kept at 500 °C for 5 min in a vacuum ($5{\cdot}10^{-3}$ Pa). Then, the tests were conducted either in a vacuum, with a maximum pressure of $3{\cdot}10^{-2}$ Pa at high temperatures, or under a protective Ar atmosphere. The samples were heated up to the maximum temperature of 1670 °C, followed by the dwell of 5 min. The heating of the samples from the temperature of 500 °C to the final testing temperature was done within 400 s (i.e. heating rate was 3 °C/s). The oxygen partial pressure in the chamber, PO_2, is dictated by the equilibrium imposed by the graphite constituting the experimental chamber. Considering the reactions involving C and O_2 and the purity of the gas used (H_2O, O_2 < 0.5 ppm), the PO_2 level did not exceed $2{\cdot}10^{-15}$ Pa at the maximum testing temperature. The whole wetting process was continuously recorded by a CCD camera connected to acquisition and calculation software, which allows the samples to be observed and the contact angles to be measured.

The wetting behaviour was evaluated by the measurement of a contact angle (θ) and drop dimensions (height and base diameter) using the sessile-drop technique [30]. The ad hoc designed ASTRAView image analysis software was used to obtain surface tension, drop dimensions and contact angle data during each experimental run [31].

2.4. Characterisation of the samples after wetting tests

The microstructures of the samples were characterised using SEM equipped with EDX (AURIGA Compact, Zeiss) on the polished cross sections of the wetted couples (using a final 1 μm diamond suspension). When the alloy detached from the substrate upon cooling down from the testing temperature, it was placed back onto the surface and glued at the previous position.

The crystalline phases in the samples after the wetting tests were determined by the XRD analysis (Panalytical Empyrean, Cu Kα radiation) of the top surfaces of the alloys in the range of 2θ from 20° to 80°. The individual phases present in the samples after wetting tests were then identified taking into account the results of both XRD and EDX analysis.

3. Results

3.1. Wetting of molten $ZrSi_2$ on CVD-SiC and C_f/SiC substrates in different atmospheres

Table 1 shows a summary of the contact angles of the $ZrSi_2$ pellets in contact with the CVD-SiC and C_f/SiC substrates, while Fig. 2 shows the high temperature contacts of the wetting couples after 5 min at 1670 °C in a vacuum or argon atmospheres. As can be seen in Fig. 2, incomplete melting of the pellets occurred in all cases, so the liquids did not reach the shape of an equilibrium drop according to the Young's law. Therefore, the final contact angles reported here must be referred as apparent contact angles [32]. Moreover, for several samples, no liquid in contact with the solid surface was observed, so no contact angles were measured.

During the high-temperature tests of pure $ZrSi_2$ in contact with the CVD-SiC substrates, the formation of a liquid at about 1620 °C was observed, but a part of the metal remained solid even after the temperature was increased to 1670 °C, followed by the dwell of 5 min. The same situation occurred in both vacuum and argon atmospheres as can be seen in Fig. 2a and b, respectively. In both cases, the liquid spread over the CVD-SiC surfaces with a contact angle well below 90°, but the use of argon led to a lower contact angle (38°), when compared to the test done in a vacuum (50°). A very similar contact angle (39°) was also measured for the non-reactive wetting of Si-10Zr alloy on SiC substrate at the temperature of 1450 °C in argon [20].

Unlike the CVD-SiC substrate, no liquid phase formation was observed when the $ZrSi_2$ pellets were tested on the surface of C_f/SiC-I3 at 1670 °C for 5 min in a vacuum (Fig. 2c) or argon (Fig. 2d). Therefore, no contact angle was measured for this substrate (Table 1). Despite the absence of any liquid on the surface, the in-situ observation during the tests showed that the height of $ZrSi_2$ pellets decreased while the diameter of the pellet remained constant (*see the video of the wetting of $ZrSi_2$ on C_f/SiC-I3 in Ar in the supplementary material*). This suggests that the

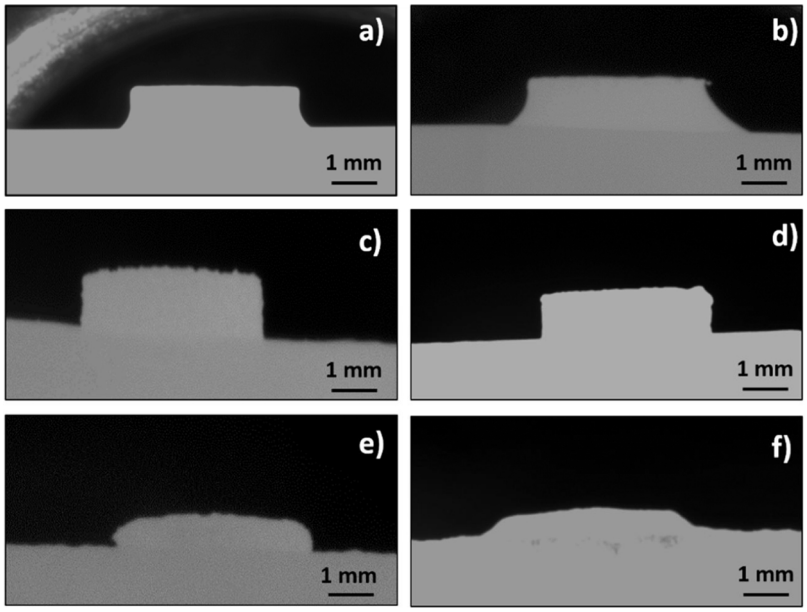

Fig. 2. Pictures of the pure $ZrSi_2$ pellets after 5 min at 1670 °C in contact with CVD-SiC in: a) vacuum, b) argon; C_f/SiC-I3 in c) vacuum, d) argon; C_f/SiC-I6 in e) vacuum, f) argon.

infiltration of the alloy into the composite occurred during the test [19]. Upon cooling from the testing temperature, the alloy detached from the C_f/SiC-I3 substrate. The same behaviour (shrinkage of the pellet with the absence of the liquid on the surface) was also observed when the C_f/SiC-I6 substrate was tested in vacuum, Fig. 2e. However, a completely different situation occurred when the wetting test of pure $ZrSi_2$ on the C_f/SiC-I6 sample was performed at 1670 °C for 5 min in argon. The alloy melted and spread over the surface of the composite, Fig. 2f (*also see the video of wetting of $ZrSi_2$ on C_f/SiC-I6 in Ar in the supplementary material*). This all led to the far best wetting and spreading behaviour of the alloy among all of the investigated substrates, leading to the lowest apparent contact angle of 23° (Table 1). In this case, the $ZrSi_2$ pellet was strongly attached to the surface of C_f/SiC-I6 after the wetting tests in both atmospheres. The reason of such different behaviour of the alloy when two different CMCs were applied will be analysed and discussed below.

Fig. 3 shows the back-scattered SEM micrographs of the cross-sections of the wetting couples after the tests conducted at 1670 °C for 5 min in a vacuum or argon. In the case of C_f/SiC-I3 sample, the alloy had to be glued to the composite surface in order to observe the interaction of the alloy with the matrix. The SEM analysis revealed that molten $ZrSi_2$ uniformly infiltrated into the C_f/SiC-I3 body, leaving behind an extremely porous alloy on the surface of the substrate. This occurred in both the vacuum (Fig. 3a) and argon (Fig. 3b) atmospheres. Although the same phenomenon was observed regardless the atmosphere, a slightly better infiltration (up to ~ 1020 μm) and a more porous alloy was observed in a vacuum atmosphere (Fig. 3a) than in argon (Fig. 3b). A worse infiltration in argon compared to vacuum is usually observed due to gas entrapment within the pores of the composite [33]. When the C_f/SiC-I6 substrate was used, molten $ZrSi_2$ infiltrated into the similar distance as occurred for the C_f/SiC-I3 sample, but this time no homogenously infiltrated sub-surface region was achieved neither in a vacuum (Fig. 3c) nor in argon (Fig. 3d). Therefore, a significantly lower amount of the alloy infiltrated into the C_f/SiC-I6 composites when compared to the C_f/SiC-I3 substrates, resulting in a less porous solidified alloy on the surface. In this case, the infiltration was suppressed due to significantly lower open and overall porosities of the C_f/SiC-I6 substrate. Since the solidified remaining alloy was strongly attached to the surface of C_f/SiC-I6 when tested in both atmospheres, chemical interactions between molten $ZrSi_2$ and C_f/SiC-I6 substrate could be investigated in more details.

Fig. 4a and b show the back-scattered SEM micrographs of the interface between $ZrSi_2$ and C_f/SiC-I6 after the tests performed in a vacuum and argon, respectively. The solidified alloy after the test in a vacuum contained some light grey phase (Fig. 4a), which are also highlighted by arrows in Fig. 3c. Such a phase was not detected in the alloy after the test in argon (Fig. 4b and 3 d). The EDX point analysis (shown in the supplementary material, Fig. S1) revealed that the light grey phase contained Zr and Si, but the amount of Si was lower than in the surrounding matrix. This indicated the presence of ZrSi phase in the matrix of remaining unreacted $ZrSi_2$ alloy. A comparison of the XRD patterns of the alloys after the test conducted in a vacuum and argon is shown in Fig. 5a. It is obvious that only ZrSi and ZrC phases were detected after the wetting test in vacuum (but some unreacted $ZrSi_2$ could be found by SEM; see above), while $ZrSi_2$ and ZrC phases were present after the test in argon. This clearly confirmed the formation of ZrSi during the high temperature interactions between the $ZrSi_2$ pellet and the C_f/SiC surface at 1670 °C in a vacuum. The EDX analysis (*see the supplementary material, Fig. S1*) also showed that the reactively formed ZrC grains were mainly located in the solidified alloy close to the interface with the composite, but also as single phase layers in the infiltrated zone of the composite (not shown here). Fig. 4b shows that the amount of ZrC grains in the solidified alloy decreased with the increasing distance from the substrate (see the inset in Fig. 4b). Regardless the atmosphere, quite a large volume of free Si (*EDX result is shown in the supplementary material, Fig. S1*) was also present in the solidified alloy, Fig. 4.

The formation of ZrSi during the test in a vacuum can be explained as follows. According to the binary Si-Zr phase diagram [34], $ZrSi_2$ undergoes a peritectic reaction at 1620 °C, which forms a Si-rich liquid (75 at.% of Si) and ZrSi (solid). However, it was reported that the evaporation of Si from Zr-Si alloys may occur under a vacuum [21]. This was confirmed in the present work, as the weight change of the $ZrSi_2$ alloy before and after the tests in a vacuum was about 12 wt.%, while only a marginal change (~ 1 wt.%) was observed for the same sample when tested in argon. The evaporation of Si in the present work can be explained by a relatively high vapour pressure (2 Pa) of pure Si at the temperature of 1670 °C [35], when compared to a vacuum in the chamber during the tests ($< 3.10^{-2}$ Pa). Similar observations were reported for the wetting of molten eutectic Si-Zr alloy on the carbon and

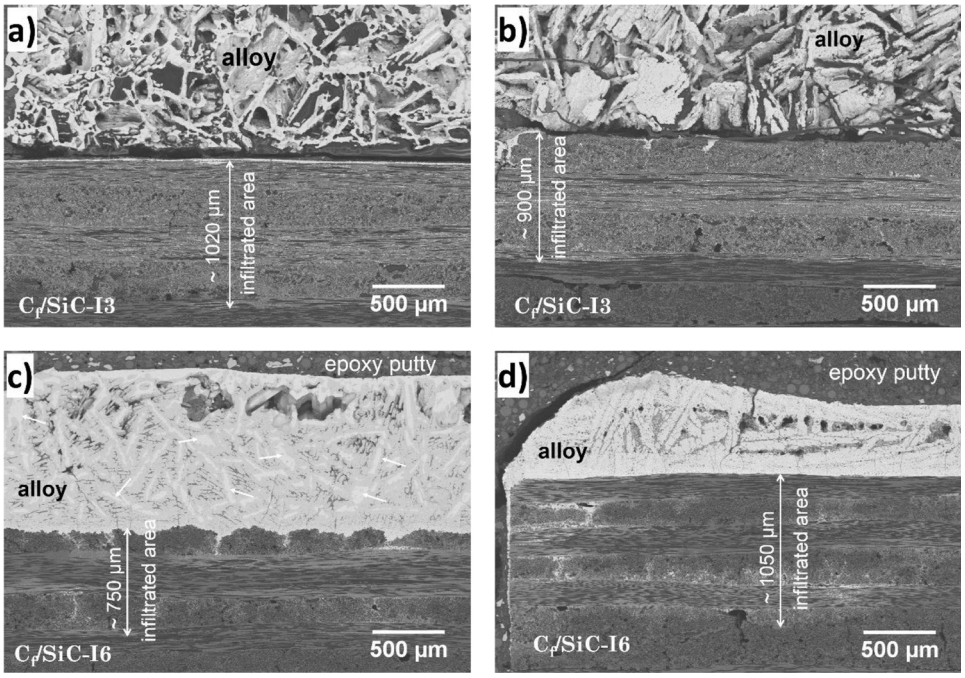

Fig. 3. Back-scattered SEM microstructures of the cross sections of $ZrSi_2$ on: C_f/SiC-I3 substrate after the wetting experiments done at 1670 °C for 5 min in a) vacuum, b) argon; or C_f/SiC-I6 substrate after a test in c) vacuum, b) argon.

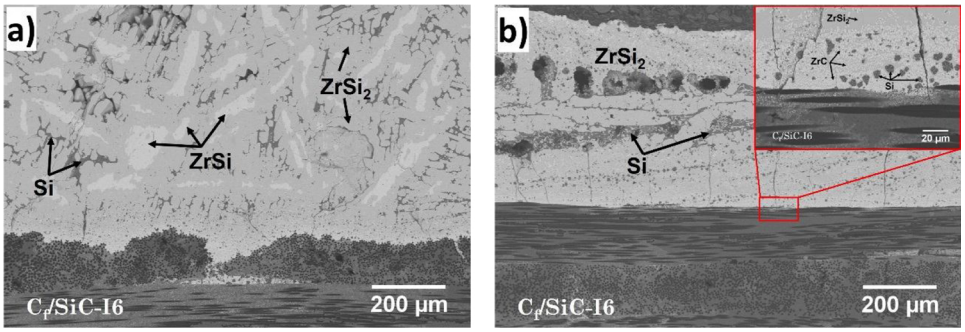

Fig. 4. Back-scattered SEM micrographs of the interface between $ZrSi_2$ and C_f/SiC-I6 after the wetting tests at 1670 °C for 5 min in a) vacuum, or b) argon. The inset shows the interface at a higher magnification, confirming the formation of ZrC.

SiC substrates [21], or for the test of molten Si-10Zr alloy in contact with SiC [20]. The evaporation of Si affected wetting and spreading behaviour of the alloy in a vacuum, leading to a slightly higher contact angle than the one measured in argon (Table 1). When the temperature was increased up to 1670 °C during the wetting experiments in a vacuum, the overall composition of the metallic phase was enriched by Zr due to the evaporation of Si. This shifted the equilibrium and left behind a large part of solid ZrSi, as was observed by SEM analysis after the high-temperature tests (Fig. 4a), and confirmed by the XRD analysis (Fig. 5a). At the same time, the interfacial reaction of the Zr-rich liquid phase with SiC occurred and, according to the isothermal section at 1600 °C of the ternary C-Si-Zr phase diagram proposed by Chen [36],

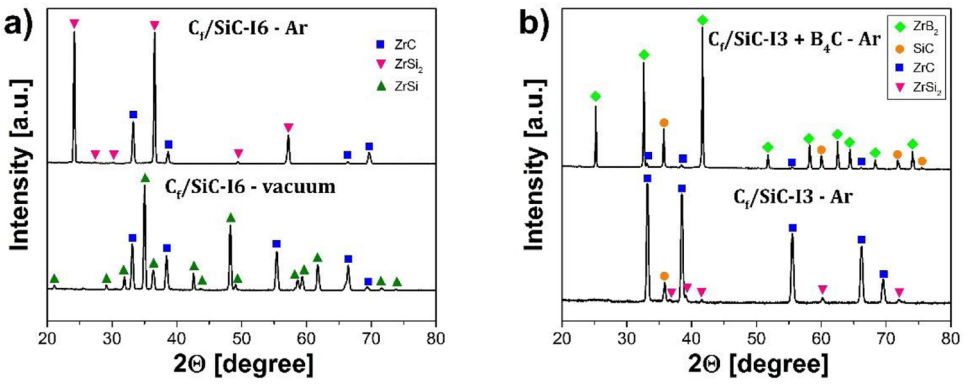

Fig. 5. a) Comparison of the XRD patterns of the top surfaces of solidified alloy on the C_f/SiC-I6 substrates after a wetting test done at 1670 °C in vacuum and argon; b) XRD patterns of the top surface of C_f/SiC-I3 and B_4C-infiltrated C_f/SiC-I3 samples after a wetting test at 1670 °C in argon.

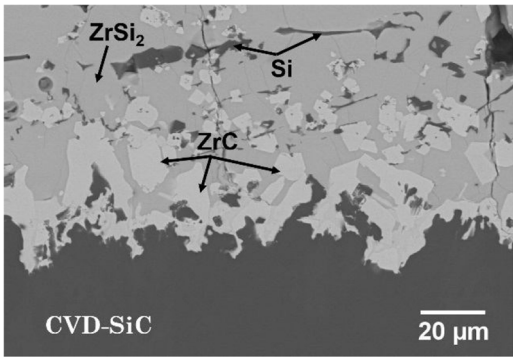

Fig. 6. Back-scattered SEM micrograph of the interface between $ZrSi_2$ and CVD-SiC after a wetting test at 1670 °C for 5 min in argon.

the ZrC_x phase and a Si-rich liquid are formed in equilibrium with SiC. This is the reason why a significant amount of the solidified Si was also observed in the alloy, further away of the interface with the substrate (Fig. 4).

When the wetting test was performed in argon, no extensive evaporation of Si occurred, so no solid ZrSi was formed. However, the $ZrSi_2$ liquid reacted with the matrix to form ZrC phase, leaving behind quite a large amount of free, unreacted Si in the alloy (Fig. 4b). Although this time a Zr-rich liquid was not formed by evaporation of Si, thermodynamic results of possible reactions showed that Zr-species of the infiltrated Zr-Si alloy have a higher reactivity than Si-species during erosion process [12]. Taking this result into account, the formation of ZrC would be expected at the interface between SiC and $ZrSi_2$. This was confirmed by the SEM analysis of the cross section of the $ZrSi_2$/SiC couple after the wetting test at 1670 °C, Fig. 6. The formation of both the ZrC phase right at the interface with SiC and the remaining solidified free Si in the alloy was clearly observed. The SEM analysis showed that the reactive wetting behaviour was observed when molten $ZrSi_2$ was in contact with the CVD-SiC substrate at the temperature of 1670 °C (Fig. 6). Despite the reactive behaviour of the alloy accompanied by dissolution of the SiC substrate in the present work, the contact angle (38°) was at the same level as the angle measured for non-reactive wetting of the Si-10Zr alloy on SiC at the temperature of 1450 °C (39°) [20].

In addition, the SEM analysis revealed a relatively significant corrosion of the surface of C_f/SiC-I6 composites after the interaction with molten $ZrSi_2$ at 1670 °C for 5 min, regardless the atmosphere (Fig. 4). On the other hand, no significant corrosion of the C_f/SiC-I3 surface was observed after the contact with the $ZrSi_2$ pellet at 1670 °C for 5 min in a vacuum or argon (Fig. 3a and b). This strongly suggests that a suppressed infiltration in the C_f/SiC-I6 composites provided a more time for the alloy to be in contact with the outer surface of the composite, leading to a more extensive reaction of the molten alloy with the substrate. On the contrary, the alloy homogenously infiltrated into the C_f/SiC-I3 composite matrix rather than reacted with its outer surface. This, along with a higher porosity of the solidified alloy, was responsible for the detachment of the alloy from the C_f/SiC-I3 surface after the wetting test, while strong chemical interactions between $ZrSi_2$ and C_f/SiC-I6 surface led to a strong adhesion.

However, a different situation was observed inside the C_f/SiC matrices. Fig. 7a and 7b show the back-scattered SEM images of the infiltrated zone in C_f/SiC-I3 and C_f/SiC-I6 matrices, respectively. It can be seen that carbon fibres were significantly eroded in the C_f/SiC-I3 matrix, as a typical circular shape of all the fibres was lost (compare Figs. 1a and 7 a). On the contrary, the shape of carbon fibres remained circular even in the highly infiltrated region of C_f/SiC-I6, although some erosion of the carbon fibres coating was observed (Fig. 7b). The SEM results suggested that a more porous SiC matrix in the C_f/SiC-I3 allowed more alloy to be infiltrated, which could more easily reach the fibres. On the other hand, a denser SiC microstructure effectively hindered alloy from coming into contact with carbon fibres in the C_f/SiC-I6 composite. In this case, the alloy reacted with a denser SiC matrix to form ZrC, which suppressed a further infiltration of the alloy towards the fibres. This was the reason of the presence of some non-infiltrated areas in the C_f/SiC-I6 composite (Fig. 7b). Such a corrosive nature of Zr-containing alloy to carbon fibres have been reported in many other works, and was considered as a typical phenomenon occurring during reactive melt infiltration process [11–14].

It can be concluded that both the atmosphere and the porosity of C_f/SiC substrates played a significant role in wetting behaviour of $ZrSi_2$. The use of a vacuum atmosphere led to the formation of solid ZrSi in the remaining, unreacted $ZrSi_2$ alloy. On the other hand, no ZrSi formation was observed when argon was used. At the same time, a significant effect of different porosities of C_f/SiC substrates was observed. The melted alloy rather infiltrated into the C_f/SiC-I3 substrate with a higher overall porosity (21 %), and no apparent melting and spreading of the alloy over the surface was observed. The infiltrated alloy formed a homogenous infiltrated sub-surface region with a thickness of ~ 1 mm, reaching both edges of the sample. The infiltrated layer was mainly composed of ZrC and some remaining $ZrSi_2$ alloy. On the contrary, significant melting and spreading of $ZrSi_2$ alloy over the surface of the C_f/SiC-I6 substrate with a lower overall porosity (12 %) was observed when tested in argon. However, a uniform infiltration of the alloy into the sub-surface layer was not observed. At the same time, the alloy extensively reacted with the composite surface, leading to a less significant erosion of both fibres and the matrix. Since no ZrSi formation and better wetting behaviour was observed when the alloy was tested in argon, this atmosphere was selected to be used for further experiments in this work.

3.2. *Wetting of $ZrSi_2$ – 5 wt.% Lu_2O_3 on B_4C-infiltrated C_f/SiC substrates*

In order to simulate the chemical interactions between $ZrSi_2$-based alloys and C_f/SiC substrates during the development of UHTCMCs with the final matrix composition of ZrB_2-SiC, the wetting tests were performed on the C_f/SiC substrates after the pressure infiltration of B_4C powder. Due to the different porosities of the starting C_f/SiC materials, a higher amount of B_4C (~ 1 wt.%) was infiltrated into the C_f/SiC-I3 substrate than into the C_f/SiC-I6 substrate (~ 0.5 wt.%). With the aim to form the final composition of ZrB_2-SiC-Lu_2O_3 with potentially improved high temperature properties, the Lu_2O_3 additive (5 wt.%) was incorporated into the $ZrSi_2$ pellets before the wetting experiments.

Similar to the wetting of pure $ZrSi_2$ on the C_f/SiC-I3 substrate, no melting and spreading of the $ZrSi_2$ -5 wt.% Lu_2O_3 alloy on the B_4C-infiltrated C_f/SiC-I3 composite was observed when tested at 1670 °C for 5 min in argon. After the test, the alloy detached from the surface of the composite, as it always happened for this substrate. On the other hand, in the case of C_f/SiC-I6 composite, a partial melting of the $ZrSi_2$ – 5 wt.% Lu_2O_3 alloy was observed without any significant spreading of the alloy over the surface (*see the wetting video of $ZrSi_2$-Lu_2O_3 on C_f/SiC-I6 + B_4C in the supplementary material)*. The melting of the alloy resulted in strong attachment of the alloy to the composite surface. Therefore, the contact angle could only be measured for the B_4C-infiltrated C_f/SiC-I6 substrate. It can be noticed that the apparent contact angle significantly increased in this case, reaching an almost double value (43°), when compared to the apparent contact angle (23°) obtained for the wetting of pure $ZrSi_2$ on the as-received C_f/SiC-I6 surface (Table 1). However, it must be pointed out that the wetting angle was still far below 90°, suggesting a good interaction between the molten $ZrSi_2$ – 5 wt.% Lu_2O_3 alloy and the B_4C-infiltrated C_f/SiC-I6 substrate.

In order to find out whether the presence of B_4C compound in the composite, or the presence of Lu_2O_3 additive in the $ZrSi_2$ alloy was responsible for a higher contact angle, a model wetting experiment of the $ZrSi_2$ – 5 wt.% Lu_2O_3 alloy on the monolithic CVD-SiC substrate (so the effect of B_4C was eliminated) was conducted at the same conditions, i.e. 1670 °C, 5 min, argon. In this case, the apparent contact angle also

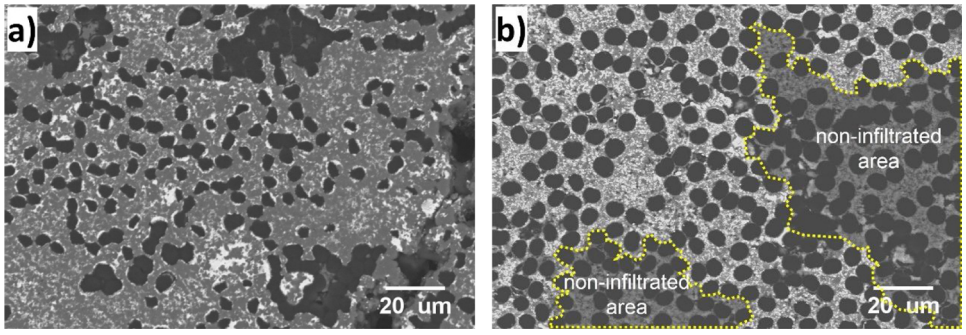

Fig. 7. Back-scattered SEM micrographs of the infiltrated region after a wetting test done at 1670 °C for 5 min in argon: a) C_f/SiC-I3 composite; b) C_f/SiC-I6 composite. The infiltrated alloy is bright, shining phase.

increased from 38° to 50°, when compared to the wetting of pure $ZrSi_2$ on the same substrate (Table 1). This clearly confirms the inhibiting effect of Lu_2O_3 particles on the wetting and spreading of molten $ZrSi_2$ on the surface of CVD-SiC at 1670 °C in argon. However, the increase in the contact angle was far less significant than in the case of C_f/SiC-I6 composite after the infiltration of B_4C, suggesting that the presence of B_4C in the composite matrix also played a role in wetting, which was investigated further by the SEM analysis.

Although the maximum infiltration of the melt into the B_4C-infiltrated C_f/SiC-I3 composite was observed up to ~ 770 µm (Fig. 8a), the spreading of the alloy inside the composite was slightly inhibited when compared to the infiltration of pure $ZrSi_2$ into the as-received C_f/SiC-I3 composite (Fig. 3a and b). This time, the infiltration of the alloy did not reach the edges of the sample, as it occurred in the previous case. After the test, the alloy detached from the surface again, leaving behind a continuous, dense outer coating layer (up to ~ 15 µm) on the surface of B_4C-infiltrated C_f/SiC-I3 sample (Fig. 8b). At the same time, the infiltrated melt filled up the micropores in the SiC matrix to form a dense sub-surface layer in the matrix, Fig. 8c. Some erosion of carbon fibres was observed again, similar to what was found in the previous case (Fig. 7). A comparison of the XRD patterns taken from the top surface of the C_f/SiC-I3 and C_f/SiC-I3 + B_4C composites after the wetting test at 1670 °C for 5 min (after the alloy was detached) is shown in Fig. 5b. The XRD results showed that while the top surface was formed mainly by ZrC and remaining unreacted $ZrSi_2$ in the case of C_f/SiC without B_4C, a desired composition in the form of ZrB_2 and SiC was found for the B_4C-infiltrated C_f/SiC-I3 matrix. Only a very small amount of ZrC was detected in this case. In addition, no unreacted $ZrSi_2$ was identified, confirming its very low amount in the composite body. Based on the XRD and SEM results, it can be concluded that the infiltrated alloy reacted with B_4C in the SiC matrix and the carbon fibres to form ZrB_2 and SiC according to the reaction (1) [37]. This was confirmed by the EDX analysis of the composite after the wetting experiment (*shown in the supplementary material, Fig. S2*). The newly formed SiC grains can be seen as well separated grains in the ZrB_2 matrix, as shown in Fig. 8c.

$$2ZrSi_2 + B_4C + 3C = 2ZrB_2 + 4SiC \quad (1)$$

$$\Delta G = -547.686 + 0.049078\,T$$

where ΔG is Gibbs free energy [KJ/mol], and T is temperature [°C].

On the other hand, no Lu_2O_3 was found in the composite body by XRD or SEM analysis. Fig. 8d shows the microstructure of the alloy, which detached from the surface of C_f/SiC-I3 composite. It is clear that

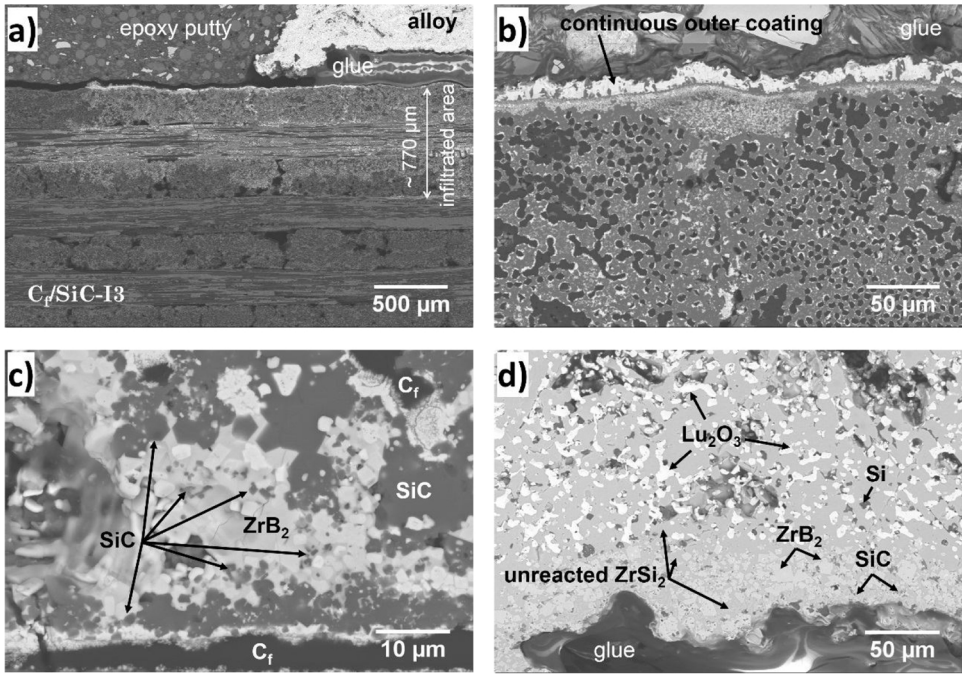

Fig. 8. Back-scattered SEM microstructures of the cross sections of $ZrSi_2$ – 5 wt.% Lu_2O_3 alloy on the B_4C-infiltrated C_f/SiC-I3 substrate after a wetting test done at 1670 °C for 5 min in Ar: a) alloy/composite interface showing the infiltration of the alloy into the composite; b) detail of the continuous outer coating followed by the infiltrated sub-surface region in the composite (the infiltrated alloy is bright, shining phase); c) detail of the in-situ formed phases in the SiC matrix of the composite; d) microstructure of the remaining alloy.

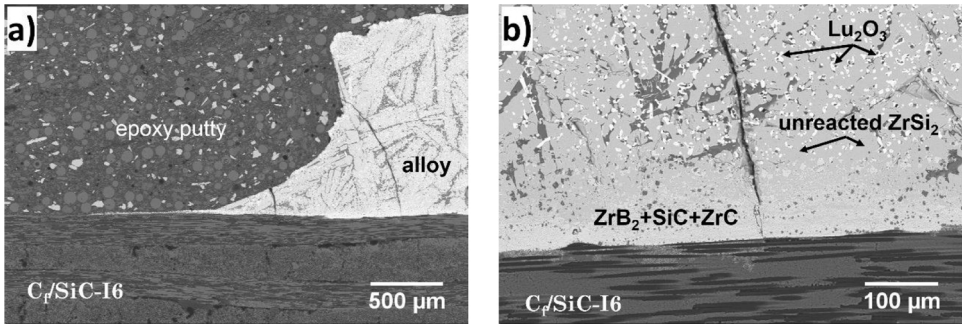

Fig. 9. Back-scattered SEM micrographs of the contact between the $ZrSi_2$ – 5 wt.% Lu_2O_3 pellet and the B_4C-infiltrated C_f/SiC-I6 substrate after a wetting test done at 1670 °C in argon: a) overview showing a limited infiltration; b) interface between the alloy and the composite.

the Lu_2O_3 particles were homogenously distributed inside the remaining unreacted $ZrSi_2$ alloy, but further from the interface with the matrix (*also see the EDX results in the supplementary material, Fig. S3*). The SEM analysis revealed two important results. Firstly, the Lu_2O_3 particles were inert and they did not react either with the alloy or the matrix. Secondly, the results indicated that the Lu_2O_3 particles were pushed away of the interface by the solidification/reaction front; similar phenomenon is commonly observed during solidification of ceramic particles reinforced Metal Matrix Composites [38]. This suggests that, besides being inert, the Lu_2O_3 particles were not wetted by the melt. Interestingly, the same situation was observed for the WC phase, which was incorporated into the alloy by ball milling process. As mentioned in the experimental part, the WC contamination was detected by XRD of the milled powder, and its amount was estimated to ~ 2 wt.%. However, no WC from ball milling was detected by the XRD analysis of the C_f/SiC-I3 surface after the wetting test (Fig. 5b). Instead, a very small amount of WC was found in the bulk of the solidified alloy, which detached from the surface (*see the EDX mapping in the supplementary material, Fig. S3*). This all indicates that, similar to the Lu_2O_3 particles, the WC phase was also inert and did not react with the alloy or the substrate, leading to its pushing away of the interaction zone towards the remaining body of the alloy.

Fig. 9 shows the back-scattered SEM micrographs of the interface between $ZrSi_2$– 5wt.% Lu_2O_3 alloy and C_f/SiC-I6 + B_4C composite after the wetting test at 1670 °C in argon. Despite the melting and partial spreading of the alloy over the top surface, no significant infiltration of the alloy into the composite body was observed (Fig. 9a). However, some corrosion of the top surface when in contact with the molten alloy was observed (Fig. 9a and b); similar to the previous case when pure $ZrSi_2$ on the composite substrates without B_4C was used (Fig. 4). Such a strong chemical interaction of the alloy with the B_4C – infiltrated C_f/SiC-I6 substrate prevented the detachment of the remaining solidified alloy from the composite surface. On the contrary, no significant corrosion of the surface of the C_f/SiC-I3 + B_4C composite was observed (Fig. 8). The microstructure of the solidified alloy after the contact with the C_f/SiC-I6 substrate consisted of the same phases as found for the C_f/SiC-I3 substrate. Again, the Lu_2O_3 particles were pushed away from the interface by the solidification/reaction front, Fig. 9b. In other words, the Lu_2O_3 particles did not affect chemical reactions between the alloys and the substrates, but stayed homogenously distributed in the remaining unreacted $ZrSi_2$ alloy. The same behaviour was observed for the test of $ZrSi_2$ – 5 wt.% Lu_2O_3 on the monolithic CVD-SiC substrate, but this time the reaction layer consisted of pure ZrC. The presence of the homogenously distributed Lu_2O_3 particles outside the reaction zone was the only difference when compared to Fig. 6; therefore, the SEM micrograph is not shown here.

It needs to be pointed out here that the motivation of adding Lu_2O_3 into the materials was to improve the oxidation/ablation resistance of composites. Taking this motivation into account, the presence of Lu_2O_3 particles in the upper parts of the solidified alloy may look advantageous, as this part of the alloy would be exposed to oxidizing environment first. On the other hand, the effect of Lu_2O_3 particles on both wetting and infiltration could significantly change when an appropriate amount of the $ZrSi_2$-based alloy would be uniformly distributed in the form of a homogenous coating on the surface of C_f/SiC. This is an ongoing work and will be published separately, along with the mechanical properties of the final UHTCMC composites.

It can be concluded that the porosity of the C_f/SiC matrix played a significant role in wetting and infiltration of the $ZrSi_2$-based alloys into the composites. The C_f/SiC-I6 material with lower overall (~ 12 %) and open (~ 9 %) porosities showed significantly better wetting behaviour than the C_f/SiC-I3 composite with higher overall (~ 21 %) and open (~ 18 %) porosities. The alloy obviously melted and the contact angle could be measured only in the case of C_f/SiC-I6 samples. On the other hand, no apparent melting and spreading of the alloy over the top surface occurred in the case of C_f/SiC-I3 substrates. When the interactions of the outer surface of the composites with $ZrSi_2$-based alloys at high temperatures are considered, the C_f/SiC composite with a lower porosity (I6) seemed to be superior to the C_f/SiC-I3 composite with a higher porosity. However, the remaining unreacted $ZrSi_2$ alloy strongly adhered to the surface of the composite, which can have a negative effect on the high temperature properties of the materials.

On the other hand, when the results of infiltration are taken into account from the point of view of developing new types of UHTCMCs, the opposite conclusion can be made. A higher porosity of C_f/SiC (I3) was beneficial for both the infiltration of B_4C into the composite body and the infiltration of the molten alloy into the B_4C-infiltrated C_f/SiC. Moreover, in the case of C_f/SiC-I3 sample, the remaining unreacted alloy was detached from the surface of the composite on its own. This resulted in the formation of a dense, continuous ZrB_2-SiC outer layer with a thickness of ~ 15 µm, followed up by the infiltrated region up to the thickness of ~ 770 µm. In the infiltrated region, the presence of ZrB_2, SiC and a very limited amount of unreacted $ZrSi_2$ was confirmed to filled up the micropores in the SiC matrix. In this way, the desired UHTCMCs composition in the upper part of the C_f/SiC composites (up to ~ 800 µm) was formed. This is believed to improve high temperature mechanical properties of C_f/SiC composites [6–11], as the high temperature properties would not be affected by the presence of a significant amount of unreacted $ZrSi_2$ (as in the case of C_f/SiC-I6).

The present results on the investigation of wetting behaviour and high temperature interactions of molten $ZrSi_2$-alloys with C_f/SiC substrates can be found very useful for the development of final UHTCMC compositions, but their actual development was out of the scope of the present work.

4. Conclusions

This work proposed a new type of UHTCMC material, in which C_f/SiC matrices are reinforced with the in-situ formed ultra-high temperature phase ZrB_2-SiC-ZrC-Lu_2O_3. Since the process relies on the

reactive melt infiltration, the effect of different porosities of C_f/SiC and different atmospheres (vacuum or argon) on the wetting behaviour of pure $ZrSi_2$ at the temperature of 1670 °C was firstly investigated. In the next step, the wetting and infiltration behaviour of molten $ZrSi_2$ – 5 wt.% Lu_2O_3 in contact with the B_4C-infiltrated C_f/SiC substrates at the temperature of 1670 °C was studied. The following conclusions can be made:

Wetting of $ZrSi_2$ on C_f/SiC substrates:

- A significant evaporation of Si in a vacuum inhibited the wetting of the alloy and led to the formation of solid ZrSi in the remaining unreacted $ZrSi_2$ alloy.
- The molten $ZrSi_2$ alloy uniformly infiltrated into the C_f/SiC-I3 composite with a higher overall porosity (~ 21 %) up to ~ 1 mm, while a non-uniform infiltration was found for the C_f/SiC-I6 with a smaller overall porosity (~ 12 %).
- The matrix of the infiltrated area consisted of the in-situ formed ZrC-SiC composition.
- In the case of C_f/SiC-I3 composite, no significant corrosion of the surface was observed, but the carbon fibres were eroded by the molten alloy.
- A denser SiC matrix in the C_f/SiC-I6 composite suppressed the infiltration, leading to the melting and spreading of $ZrSi_2$ over the C_f/SiC composite surface with the apparent contact angle of 23°.

Wetting of $ZrSi_2$ – 5 wt.% Lu_2O_3 on B_4C-infiltrated C_f/SiC:

- A higher porosity of the matrix was beneficial for both the infiltration of B_4C slurry into the C_f/SiC composite and the infiltration of molten alloy into the B_4C-infiltrated C_f/SiC.
- While a homogenously infiltrated region was formed in the upper part (up to ~ 800 μm) of the C_f/SiC-I3 + B_4C composite, almost no infiltration of the alloy occurred in the case of B_4C-infiltrated C_f/SiC-I6 with a lower porosity. The desired UHTCMCs composition (ZrB_2-ZrC-SiC) was formed in the infiltrated region.
- The Lu_2O_3 particles were not wetted by the melt, and the solidification front pushed them away of the reaction zone towards the body of the remaining unreacted alloy.

Acknowledgement

This project has received funding from the European Union's Horizon 2020 research and innovation programme under the Marie Sklodowska-Curie grant agreement No 798651. This work was also supported by the Slovak Research and Development Agency under the contract no. APVV-17-0328 and by the MVTS project of SAS "Ultracom". The authors are very grateful to Achim Schoberth (Airbus Defence and Space GmbH) for the supply of the composite materials.

Appendix A. Supplementary data

Supplementary material related to this article can be found, in the online version, at doi:https://doi.org/10.1016/j.jeurceramsoc.2020.05.055.

References

[1] W.G. Fahrenholtz, E.J. Wuchina, W.E. Lee, Y. Zhou (Eds.), Ultra-High Temperature Ceramic Materials: Materials for Extreme Environment Applications, John Wiley & Sons, 2014.
[2] R. Savino, Aerothermodynamic study of UHTC-based thermal protection systems, Aerosp. Sci. Technol 9 (2) (2005) 151–160.
[3] L. Silvestroni, S. Mungiguerra, D. Sciti, G.D. Di Martino, R. Savino, Effect of hypersonic flow chemical composition on the oxidation behavior of a super-strong UHTC, Corros. Sci. 159 (2019) 108125.
[4] W. Krenkel (Ed.), Ceramic Matrix Composites: Fibre Reinforced Ceramics and Their Application, Wiley-VCH Verlag GmbH & Co., 2008.
[5] M.E. Westwood, J.D. Webster, R.J. Day, F.H. Hayes, R. Taylor, Review oxidation protection of carbon fibre composites, J. Mater. Sci. 31 (1996) 1389–1397.
[6] J. Binner, M. Porter, B. Baker, J. Zou, V. Venkatachalam, V.R. Diaz, A. D'Angio, P. Ramanujam, T. Zhang, T.S.R.C. Murthy, Selection, processing, properties and applications of ultra-high temperature ceramic matrix composites, UHTCMCs – a review, Int. Mater. Rev. (2019), https://doi.org/10.1080/09506608.2019.1652006.
[7] L. Zoli, D. Sciti, Efficacy of a ZrB_2-SiC matrix in protecting C fibres from oxidation in novel UHTCMC mateirals, Mater. Design 113 (2017) 207–213.
[8] A. Paul, S. Venugopal, J.G.P. Binner, B. Vaidhyanathan, A.C.J. Heaton, P.M. Brown, UHTC-carbon fibre composites: preparation, oxyacetylene torch testing and characterization, J. Eur. Ceram. Soc. 33 (2013) 423-232.
[9] L. Zoli, A. Vinci, L. Silvestroni, D. Sciti, M. Reece, S. Grasso, Rapid spark plasma sintering to produce dense UHTCs reinforced with undamaged carbon fibres, Mater. Design 130 (2017) 1–7.
[10] H. Hu, Q. Wang, Z. Chen, C. Zhang, Y. Zhang, J. Wang, Preparation and characterization of C/SiC-ZrB_2 composites by precursor infiltration and pyrolysis process, Ceram. Int. 36 (2010) 1011–1016.
[11] X. Chen, D. Ni, Y. Kan, Y. Jiang, H. Zhou, Z. Wang, S. Dong, Reaction mechanism and microstructure development of $ZrSi_2$ melt-infiltrated C_f/SiC-ZrC-ZrB_2 composites: the influence of preform pore structures, J. Materiomics 4 (2018) 266–275.
[12] X. Chen, S. Dong, Y. Kan, X. Jin, H. Zhou, D. Ni, D. Wang, Microstructure and mechanical properties of three dimensional C_f/SiC-ZrC-ZrB_2 composites prepared by reactive melt infiltration method, J. Eur. Ceram. Soc. 36 (2016) 3969–3976.
[13] Y. Wang, X. Zhu, L. Zhang, L. Cheng, Reaction kinetics and ablation properties of C/C-ZrC composites fabricated by reactive melt infiltration, Ceram. Int. 37 (2011) 1277–1283.
[14] H. Pi, S. Fan, Y. Wang, C/SiC-ZrB_2-ZrC composites fabricated by reactive melt infiltration with $ZrSi_2$ alloy, Ceram. Int. 38 (2012) 6541–6548.
[15] Y. Tong, S. Bai, Y. Ye, H. Zhang, Z. Yang, Reactive melt infiltration of a ZrB_2 modified C/ZrC composite by a eutectic Zr–B alloy, Mater. Lett. 138 (2015) 208–211.
[16] J. Jiang, S. Wang, W. Li, Z. Chen, Y. Zhu, Preparation of 3D C_f/Zr-SiC composites by joint processes of PIP and RMI, Mat. Sci. Eng. A 607 (2014) 334–340.
[17] Y. Tong, S. Bai, K. Chen, C/C–ZrC composite prepared by chemical vapor infiltration combined with alloyed reactive melt infiltration, Ceram. Int. 38 (7) (2012) 5723–5730.
[18] R. Voytovych, V. Bougiouri, N.R. Calderon, J. Narciso, N. Eustathopoulos, Reactive infiltration of porous graphite by NiSi alloys, Acta Mater. 56 (10) (2008) 2237–2246.
[19] A. Léger, L. Weber, A. Mortensen, Influence of the wetting angle on capillary forces in pressure infiltration, Acta Mater. 91 (2015) 57–69.
[20] D. Giuranno, G. Bruzda, A. Polkowska, R. Nowak, W. Polkowski, A. Kudyba, N. Sobczak, F. Mocellin, R. Novakovic, Design of refractory SiC/$ZrSi_2$ composites: wettability and spreading behavior of liquid Si-10Zr alloy un contact with SiC at high temperatures, J. Eur. Ceram. Soc. 40 (2020) 953–960.
[21] M. Naikade, B. Frankhänel, L. Weber, A. Ortona, M. Stelter, Studying the wettability of Si and eutectic Si-Zr alloy on carbon and silicon carbide by sessile drop experimens, J. Eur. Ceram. Soc. 39 (2019) 735–742.
[22] M.M. Opeka, I.G. Talmy, J.A. Zaykoski, Oxidation-based materials selection for 2000°C+ hypersonic aerosurfaces: theoretical considerations and historical experience, J. Mater. Sci. 39 (2004) 5887–5904.
[23] D.D. Jayaseelan, E. Zapata-Solvas, R.J. Chater, W.E. Lee, Structural and compositional analyses of oxidised layers of ZrB_2-based UHTCs, J. Eur. Ceram. Soc. 35 (2015) 4059–4071.
[24] E. Zapata-Solvas, D. Gómez-García, A. Domínguez-Rodríguez, W.E. Lee, High temperature creep of 20vol.%SiC-HfB_2 UHTCs up to 2000°C and the effect of La_2O_3 addition, J. Eur. Ceram. Soc. 38 (2018) 47–56.
[25] Y. Jia, H. Li, L. Feng, J. Sun, K. Li, Q. Fu, Ablation behavior of rare earth La-modified coating for SiC-coated carbon/carbon composites under an oxyacetylene torch, Corros. Sci. 104 (2016) 61–70.
[26] P. Tatarko, M. Kašiarová, J. Dusza, P. Šajgalík, Influence of rare-earth oxide additives on the oxidation resistance of Si_3N_4-SiC, J. Eur. Ceram. Soc. 33 (2013) 2259–2268.
[27] Š. Lojanová, P. Tatarko, Z. Chlup, M. Hnatko, J. Dusza, Z. Lenčéš, P. Šajgalík, Rare-earth element doped Si_3N_4/SiC micro/nano-composites – RT and HT mechanical properties, J. Eur. Ceram. Soc. 30 (2010) 1931–1944.
[28] L. Luo, J. Liu, L. Duan, Y. Wang, Multiple ablation resistance of La_2O_3/Y_2O_3-doped C/SiC-ZrC composites, Ceram. Int. 41 (2015) 12878–12886.
[29] R. Sangiorgi, M.L. Muolo, D. Chatain, N. Eusthatopoulos, Wettability and work of adhesion of nonreactive liquid metals on silica, J. Am. Ceram. Soc. 71 (1988) 742–748.
[30] Wettability at High temperatures, in: N. Eustathopoulos, M.G. Nicholas, B. Drevet (Eds.), Pergamon Materials Series, 1999.
[31] L. Liggieri, A. Passerone, An automatic technique for measuring the surface tension of liquid metals, High Temp. Technol. 7 (1989) 82–86.
[32] J.A. Warren, W.J. Boettinger, A.R. Roosen, Modeling reactive wetting, Acta Mater.

46 (1998) 3247–3264.
[33] M. Caccia, J. Narciso, Key parameters in the manufacture of SiC-based composite materials by reactive melt infiltration, Materials 12 (15) (2019) 2425–2443.
[34] H. Okamoto, The Si-Zr (silicon-zirconium) system, Bull. Alloy Phase Diagrams. 11 (1990) 513–519.
[35] P.D. Desai, Thermodynamic properties of Fe and Si, J. Phys. Chem. Ref. Data 15 (1986) 967.
[36] H.M. Chen, Y. Xiang, S. Wang, F. Zheng, L.B. Liu, Z.P. Jin, Thermodynamic Assessment of the C – Si – Zr System vol. 474, (2009), pp. 76–80, https://doi.org/10.1016/j.jallcom.2008.06.086.
[37] S.H. Lee, S.Y. Choi, H.D. Kim, ZrB_2-SiC nano-powder mixture prepared using $ZrSi_2$ and modified spark plasma sintering, J. Am. Ceram. Soc. 96 (4) (2013) 1051–1054.
[38] Y.M. Youssef, R.J. Dashwood, P.D. Lee, Effect of clustering on particle pushing and solidification behaviour in TiB_2 reinforced aluminium PMMCs, Compposites Part A: Applied Science and Manufacturing 36 (6) (2005) 747–763.